

Structure of marginally jammed polydisperse packings of frictionless spheresChi Zhang,¹ Cathal B. O'Donovan,² Eric I. Corwin,³ Frédéric Cardinaux,¹ Thomas G. Mason,^{4,5} Matthias E. Möbius,² and Frank Scheffold^{1,*}¹*Department of Physics, University of Fribourg, CH-1700 Fribourg, Switzerland*²*School of Physics, Trinity College Dublin, 2, Dublin, Ireland*³*Department of Physics, University of Oregon, Eugene, Oregon 97403, USA*⁴*Department of Chemistry and Biochemistry, University of California, Los Angeles, California 90095, USA*⁵*Department of Physics and Astronomy, University of California, Los Angeles, California 90095, USA*

(Received 29 October 2014; revised manuscript received 1 February 2015; published 2 March 2015)

We model the packing structure of a marginally jammed bulk ensemble of polydisperse spheres. To this end we expand on the granocentric model [Clusel *et al.*, *Nature (London)* **460**, 611 (2009)], explicitly taking into account rattlers. This leads to a relationship between the characteristic parameters of the packing, such as the mean number of neighbors and the fraction of rattlers, and the radial distribution function $g(r)$. We find excellent agreement between the model predictions for $g(r)$ and packing simulations, as well as experiments on jammed emulsion droplets. The observed quantitative agreement opens the path towards a full structural characterization of jammed particle systems for imaging and scattering experiments.

DOI: [10.1103/PhysRevE.91.032302](https://doi.org/10.1103/PhysRevE.91.032302)

PACS number(s): 82.70.Dd, 47.57.J-, 64.70.pv, 83.80.Iz

I. INTRODUCTION

The question of how to optimally pack objects of various shapes in space has been of fundamental interest in mathematics and physics for centuries [1,2]. It is also highly relevant for many practical problems ranging from storage and industrial packing to the properties of soft materials such as emulsions, foams, or granular materials [3–11]. Amorphous packings are particularly difficult to understand due to the complexity of disordered nonequilibrium structures. There exists a broad agreement that disordered assemblies of spheres can be driven into a solid state by filling space up to a certain critical volume fraction $\phi_c \sim 0.64$ [12,13]. At this point, denoted *random close packing* or *jamming*, the system is marginally stable. Mechanical stability is provided by an average isostatic number of contacts which in three dimensions is $\bar{Z}_J = 6$ for frictionless spheres [4,14,15]. The advent of powerful simulation techniques over the last two decades has led to numerous new results and predictions. Soft spheres can be quenched into a compressed state $\phi > \phi_c$, and many relevant physical quantities, such as the modulus or the pressure, have been predicted to scale with the excess number of contacts $\Delta Z = \bar{Z}_J - 6$ [4,14]. Despite the recent progress made, the experimental relevance of these predictions has been questioned [15]. As a matter of fact there are only a few experimental studies which attempt to verify the numerical predictions [16–18] and study their relevance with respect to bulk properties of practically relevant materials [19,20]. This is partly due to the fact that the model assumptions made, such as the interaction potential between spheres or the size distribution, do not realistically reflect the situation in experimental systems such as in emulsions, dispersions, or foams [4–6]. Another important shortcoming of numerical studies is that these are generally carried out on real-space assemblies, whereas many experiments rely on scattering techniques that operate in k space. While real-space experiments are rather

straightforward in two dimensions [16], they are much more difficult to carry out in three dimensions [17], particularly when other physical properties, such as mechanical strength or internal dynamic modes, need to be studied as well. For this case scattering techniques, often in combination with mechanical shear measurements, have long been methods of choice to study soft disordered materials in the bulk [21–24]. Although scattering methods are highly appropriate for soft systems, certain dynamic scattering methods can be highly sensitive to the rattlers in polydisperse systems, e.g., leading to ensemble-average mean square displacements that appear to relax more rapidly, compared to what would be predicted from macroscopic rheology measurements using the generalized Stokes-Einstein relation (GSER) [25] of passive microrheology. A direct comparison between numerical results and both structural as well as dynamic experiments, however, is again complicated by the idealizations made in the models. It would therefore be desirable to derive more general concepts that allow a direct comparison between experiment and theory.

In the present work we address this problem and demonstrate how to model polydisperse sphere packings, taking into account explicitly the population of mechanically unstable particles, or *rattlers*. To this end we expand on the granocentric model (GCM) introduced by Brujic and co-workers [26,27] by uniformly distributing noncontact neighbors and by taking into account size correlations between particle and shell. We show that such an extended granocentric model (eGCM) provides an accurate description of the statistical ensemble, which in turn allows the comparison to *measurable* bulk quantities such as the radial distribution function $g(r)$. The latter is one of the most important structural measures for amorphous solids that is readily observable, both in a real-space and in a scattering experiment, via the structure factor $S(k) = 1 + 4\pi\rho/k \int_0^\infty dr r \sin(kr)[g(r) - 1]$, where ρ is the particle number density [28]. The importance of this quantity has recently been pointed out when studying the vestige of the jamming transition in an experiment both in two [18] and three dimensions [29].

*Frank.Scheffold@unifr.ch

II. THE EXTENDED GRANOCENTRIC MODEL

The granocentric model addresses the packing problem from the perspective of a single particle. The statistical properties of the local packing structure are obtained by the random formation of nearest neighbors in a one-dimensional model [26]. By numerical evaluation predictions are made about the number of neighbors and contacts as well as the local packing fraction of polydisperse spheres at random close packing. Built upon the original model, an improved version, denoted GCM 2.0 [27], was introduced by the same group soon after. The latter can also be applied to monodisperse systems while the original one could not. Despite these improvements the GCM 2.0 still does not allow predictions to be made readily about bulk quantities such as the radial distribution function.

To overcome this limitation, in our eGCM we explicitly take into account rattlers and introduce some improvements to the model as outlined in the following. We divide the particles into two groups, mechanically stable jammed particles and freely floating rattlers, then take averages over a representative set of all particles rather than considering only particles in contact. We first consider the probability of finding a central particle with radius a which is equal to particle size distribution $p(a)$. The polydispersity $PD = \delta a / \bar{a}$ is defined by the standard deviation δa of $p(a)$ divided by its mean $\bar{a} = \int a p(a) da$. For the probability to find a neighboring particle of a certain size $p_2(a)$, we explicitly consider the influence of size correlations between particles and their shell, previously neglected [26]. Packing simulations suggest [30]

$$p_2(a) \propto p(a)[1 + (a/\bar{a})^2], \quad (1)$$

which we are using here. Next we address the distribution $G_s(s)$ of surface-to-surface separations $s = r - 2a$. The latter has to be modeled independently for the stable particles and for the rattlers. We can use the scaling of the excess number of contacts $\Delta Z \sim \sqrt{Z_J - 6}$ to derive $G_{s,J}(s) \sim s^{-1/2}$ [31]. For the rattlers we take the simple *ad hoc* assumption that their neighbors are distributed uniformly, $G_{s,R} = \text{const}$. The shell of neighbors is bounded by a cutoff distance s_{cutoff} . Here, we label particles that are in contact with J and particles that are rattlers with R ; if labels J or R do not appear, then we are referring to all particles. The eGCM can be evaluated numerically and we can obtain statistical information directly from the model. However, a more general approach would be to reduce the discussion, e.g., of the radial distribution function, to its dependence on a small set of characteristic parameters, such as the average number of neighbors (\bar{N}_J, \bar{N}_R) of jammed or rattling particles, the fraction of rattlers q , and the distance s_{cutoff} . To this end we can write

$$g(r) = \frac{1}{4\pi r^2 \rho} \int f(x) G_s(r-x) dx, \quad (2)$$

where $f(x) = \int p(a) p_2(x-a) da$ is the probability of finding a central particle with radius a and another neighboring particle with radius $x-a$, for all possible a and $G_s(s) = (1-q)G_{s,J}(s) + qG_{s,R}(s)$. The link to the average number of neighbors is established by normalization via $G_{s,R}(s) = \bar{N}_R / s_{\text{cutoff}}$ and

$$G_{s,J}(s) = \begin{cases} 6\delta(0) & (s=0), \\ \frac{1}{2}(\bar{N}_J - 6)(s_{\text{cutoff}}s)^{-\frac{1}{2}} & (s>0). \end{cases} \quad (3)$$



FIG. 1. (Color online) Granocentric model. Modeling the shell of first neighbors of a central particle with radius a_c using a one-dimensional statistical approach. Particles with radius a are drawn randomly from a distribution $p_2(a)$ and added one after another as explained in the text. The solid angles occupied by the already added particles are shown as colored blocks. The remaining accessible solid angle for subsequent additions is denoted Ω_a . The dashed line indicates the threshold solid angle Ω_{max} .

The numerical implementation of our eGCM is guided by the original work [26,27], albeit with some modifications. In practice we start by considering a particle that is closely surrounded by neighbors. The size of this central particle is randomly chosen from the size distribution function $p(a)$. The solid angle occupied by a neighbor can be characterized by:

$$\omega = 2\pi \left(1 - \sqrt{1 - \left(\frac{a}{a + a_c + s} \right)^2} \right), \quad (4)$$

where a_c and a are the radii of the central particle and the neighboring particle, respectively, and s is again the surface-to-surface separation. For a given central particle, its neighbors cannot fill up the whole solid angle 4π due to geometrical constraints [26]. We thus introduce a threshold solid angle as Ω_{max} , as illustrated in Fig. 1.

Neighbors are added one at a time, with sizes randomly chosen from the size distribution of neighbors $p_2(a)$. The probability that an added neighbor is in contact with the central particles is assumed to be

$$c = \alpha \left(\frac{\Omega_a}{\Omega_{\text{max}}} \right)^{\frac{3}{2}}, \quad (5)$$

where Ω_a is the accessible solid angle and α is an adjustable prefactor. Noncontact neighbors are placed according to Eq. (3). Then neighbors are added consecutively until the total solid angle exceeds the threshold Ω_{max} . In half of the cases, chosen randomly, we either add or remove the last added neighbor with equal probability.

Relation (5) in our model can be motivated as follows: Using a constant probability of contact (as it was done in Ref. [26]) will lead to an overestimation of the fraction of rattlers. This can be seen when considering a monodisperse system with an average number of ~ 14 neighbors. This implies for the contact ratio $c = 6/14 \simeq 0.43$ and we can easily calculate the ratio of rattlers (particles with $Z < 4$) by summing the probabilities of having only $Z = 0, 1, 2$ or 3 contacts

$$q = (1-c)^{14} + \binom{14}{1}(1-c)^{13}c + \binom{14}{2}(1-c)^{12}c^2 + \binom{14}{3}(1-c)^{11}c^3 = 0.084, \quad (6)$$

where $\binom{n}{k}$ is the combination operator. This value is distinctively higher than the value for monodisperse packings observed in packing simulations, known to be of the order

of $\sim 2\%$ [30]. Using the probability of contact given by Eq. (5), however, we find excellent agreement with packing simulations, both for monodisperse and polydisperse packings, as shown later in the text. For the numerical evaluation of the eGCM, a limited set of input parameters is taken from packing simulations [30]. The latter suggest isostatic values $\bar{N}_J = 14.3$ and $\phi_c^J = 0.62$ for the jamming volume fraction of spheres in contact, independent of polydispersity [30,32]. Shells are filled up to a maximum solid angle Ω_{\max} , treated as an adjustable parameter in the numerical evaluation of the model. We generate 50 000 neighboring shells following the generic approach of Refs. [26] and [30]. Central particles with a contact number $Z < 4$ are considered as rattlers and all their neighbors are redistributed uniformly. \bar{Z}_J is obtained by taking the average over all central particles with $Z \geq 4$. We adjust $\alpha, s_{\text{cutoff}}$, and Ω_{\max} until \bar{Z}_J, \bar{N}_J , and ϕ_c^J converge towards their isostatic values and thus obtain predictions for N, Z, q , and ϕ_c . Moreover, we find $s_{\text{cutoff}}/\bar{a} \in [0.75, 1]$ and $\Omega_{\max} \in [3.33\pi, 3.53\pi]$ (see also Ref. [26]). To calculate the volume fraction ϕ directly from the eGCM results, we follow the approach introduced in Ref. [26]. For each neighbor, a cone is formed by its corresponding solid angle. Using the Voronoi radical tessellation surface at the bottom of this cone, a corresponding volume can be calculated. Summing up all neighbors of a central particle i , the cell volume V_{cell}^i is obtained. Since the actual total solid angle $\Omega_{\text{total}} < 4\pi$, we use $V_{\text{cell}}^i \frac{4\pi}{\Omega_{\text{total}}}$ as the total cell volume of the i th particle. Thus the volume fraction can be written as

$$\phi = \frac{\sum_i V_{\text{particle}}^i}{\sum_i V_{\text{cell}}^i \frac{4\pi}{\Omega_{\text{total}}}}. \quad (7)$$

III. EXPERIMENTS

We compare the model predictions with experiments on micron-scale emulsion droplets under marginal jamming conditions. For the experiments we prepare a 3:1 mixture by weight of polydimethylsiloxane (PDMS) and silicone oil (AR200) and emulsify it with sodium dodecyl sulfate (SDS) surfactant in water by shearing in a custom-made Couette shear cell. Stabilized with SDS, the droplets are fractionated by size using depletion sedimentation [33]. The size segregation is repeated until the desired polydispersity is reached. Subsequently the surfactant SDS is exchanged by the block-copolymer surfactant Pluronic F108, in order to sterically stabilize the droplets. Finally, formamide and dimethylacetamid (DMAC) are added to the solvent in order to match the density and refractive index simultaneously under experimental conditions at room temperature $T = 22^\circ\text{C}$. Optical contrast between the droplets and the dispersion medium is obtained by adding the fluorescent dye Nile red. Although the dye is present both in the solvent and the oil, the emission spectra are different, which allows one to clearly distinguish both phases, as shown in Fig. 2(a). The particle size and polydispersity are obtained from wide-field microscopy. For the polydispersities considered we find the size distribution of the emulsion droplets to be close to log-normal. Equally, simulation data and the eGCM are evaluated for two-parameter log-normal size distributions. Here we include experimental data for three droplet radii:

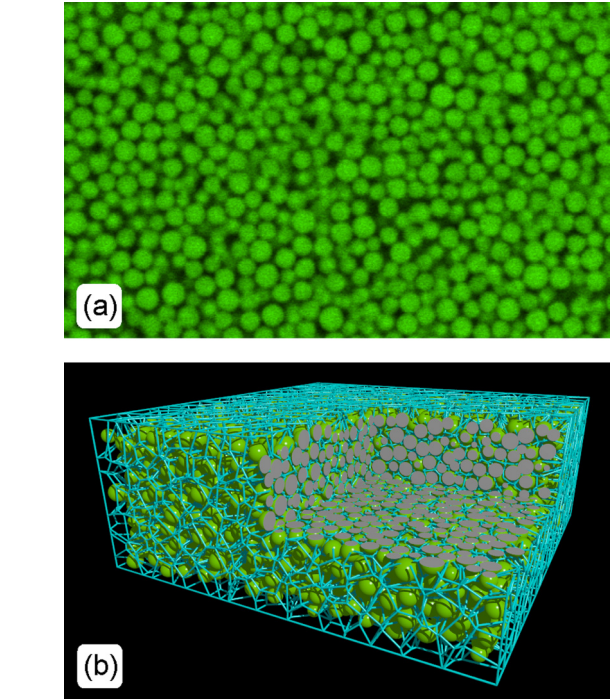


FIG. 2. (Color online) Three-dimensional imaging of jammed emulsions droplets with an average droplet radius $\bar{a} = 1.05 \mu\text{m}$. (a) Raw image of a plane in the bulk of the sample obtained by laser-scanning confocal microscopy of light emitted by the fluorescent dye Nile red at $\lambda = 595 \text{ nm}$. The droplets are marginally jammed and the volume fraction is $\phi \simeq 0.646 \pm 0.014$. (b) 3D reconstruction of the droplet positions using the sphere-matching method (SMM). The lines show the Voronoi radical tessellation around the droplet centroids. The total dimensions are $51.2 \times 51.2 \times 20.1 \mu\text{m}$. One corner is cut out to reveal the internal structure of the jammed system.

$\bar{a} = 1.1 \mu\text{m}$ with a polydispersity $\text{PD} = 0.105$, $\bar{a} = 1.07 \mu\text{m}$ with a polydispersity $\text{PD} = 0.12$, and $\bar{a} = 1.05 \mu\text{m}$ with a polydispersity $\text{PD} = 0.147$, respectively. By lowering the temperature to 4°C , a slight density mismatch is induced and the sample can be spun down to densities at and above jamming. Several hundred microliters of the jammed sample are placed in a cylindrical cell tightly connected with UV-curable glue to a microscope cover slip which allows imaging from below in an inverted microscope. High-resolution images of the individual droplet positions are obtained using three-dimensional (3D) laser-scanning confocal microscopy (A1R, Nikon, Japan). The dye is excited with a 488-nm laser line and two emission channels (525 ± 50 and $595 \pm 50 \text{ nm}$) are recorded simultaneously to improve the quality of the analysis. 3D images of size $512 \times 512 \times 201$ pixels are recorded with a resolution of 100 nm/pixel in all spatial directions. For every stack of images, the acquisition time is 100 s. To track the position of the polydisperse droplets, we implement the sphere-matching methods (SMMs) algorithm [34]. A Voronoi radical tessellation is applied and particles with adjacent cell walls are identified as neighbors [Fig. 2(b)]. We find the lateral position accuracy to be approximately 15 nm and axial accuracy 30 nm . In order to identify the point of marginal jamming, the sample is diluted in steps of $\sim 0.5\%$ in volume fraction. From a time series of two-dimensional (2D) images

we can easily identify the liquid-to-solid transition, that in our case sets the jamming volume fraction ϕ_c . From the droplet positions in 3D we calculate the radial distribution function $g(r)$ and take an average of over 20 image stacks in order to improve the statistical accuracy.

IV. RESULTS AND DISCUSSION

We first compare the eGCM predictions (squares) to simulations (circles) of disordered packings of spheres as shown in Fig. 3. Details of the simulations are discussed elsewhere [30]. Briefly, spheres are placed at random in a 3D periodic cell and the size of the spheres is drawn from the distribution $p(a)$. The sphere sizes are then increased in unison until the desired packing fraction ϕ_c is reached. Spheres are assumed to interact through purely repulsive body-centered forces and the overlap between two particles in contact leads to a harmonic interaction potential. A conjugate gradient method

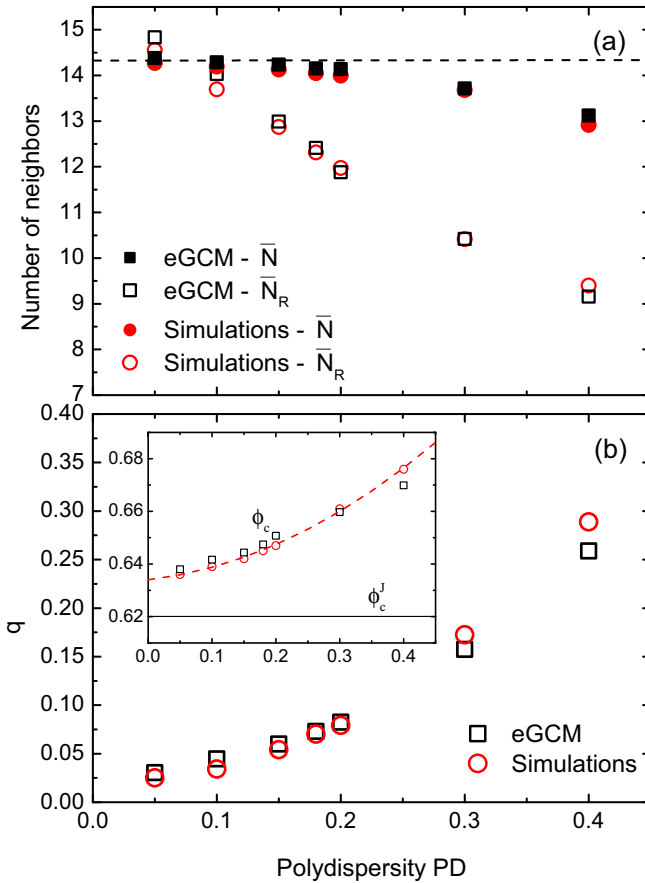


FIG. 3. (Color online) (a) Average number of first-shell neighbors \bar{N} of jammed particles (full symbols) and rattlers (open symbols) versus polydispersity (PD). Squares denote the results from the extended granular model (eGCM) and circles show the data from numerical simulations. The dashed line indicates a constant value of $\bar{N}_R = 14.3$. (b) Fraction of rattlers q predicted by the eGCM (open squares) and from simulations (open circles). Inset: Predicted jamming volume fraction ϕ_c for all particles as a function of polydispersity. Dashed line: parabolic fit $\phi_c = (0.634 + 0.0278)PD + (0.196)PD^2$. Solid line: jamming volume fraction for particles in contact $\phi_c^J = 0.62$.

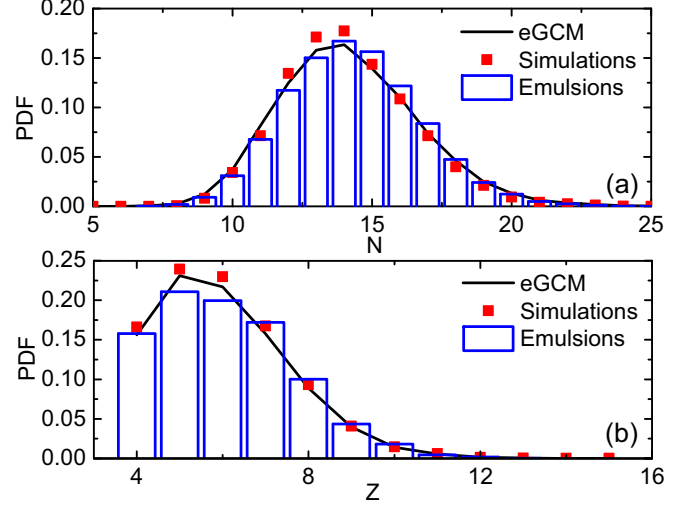


FIG. 4. (Color online) Probability distribution functions as a function of (a) number of nearest neighbors N and (b) number of contacts Z for a polydispersity $PD = 0.15$. Solid line: eGCM; squares: simulations; bars: experiments on emulsion droplets with an average droplet radius $\bar{a} = 1.05 \mu\text{m}$. The eGCM and the simulations assume a log-normal size distribution. The size distribution of the emulsion is also close to log-normal with $PD \simeq 0.15 \pm 0.01$.

is used to minimize the overlap between spheres and hence the total energy of the packing [35].

Figure 3 shows the average values \bar{N} , \bar{N}_R , and q as a function of polydispersity. We note immediately that \bar{N}_R rapidly decreases with polydispersity. This can be explained by the fact that with increasing polydispersity more rattling configurations are created by placing large particles next to a central particle. Since large particles occupy a more solid angle, fewer neighbors can be placed around a rattler and thus \bar{N}_R decreases. Equally good agreement is obtained for the average number of neighbors \bar{N} , \bar{N}_R , the fraction of rattlers and the jamming volume fraction (Fig. 3 and inset). In Fig. 4 we show the results obtained for the probability distribution of the number of neighbors N and contacts Z for a typical polydispersity of $PD = 0.15$. The experimental results are in excellent agreement with both the packing simulations and the eGCM model.

In Fig. 5(a) the model predictions for the radial distribution function are compared to the $g(r)$ derived from the experimental droplet positions. While for perfectly monodisperse packings the peak value g_1 should diverge at the jamming transition, this divergence is avoided for a size distribution of finite width. We find nearly quantitative agreement between all three data sets. Small deviations between the experimental $g(r)$ and the numerical predictions can be attributed to the limited accuracy in the experiment when determining the exact location of the particles [36]. Also, the prediction by Eq. (2) becomes less accurate as r approaches $s_{\text{cutoff}} + 2\bar{a}$. Extracting the peak value g_1 shows excellent agreement over a broad range of PD values, as shown in Fig. 5(a). Moreover, we include a data point obtained for 3D assemblies of microgel particles with a mean size $\bar{a} \simeq 0.5 \mu\text{m}$ and a $PD \leq 0.1$ taken from [29] and again find excellent agreement. Equally good agreement is obtained for the width of the first peak, as shown in Fig. 5(b).

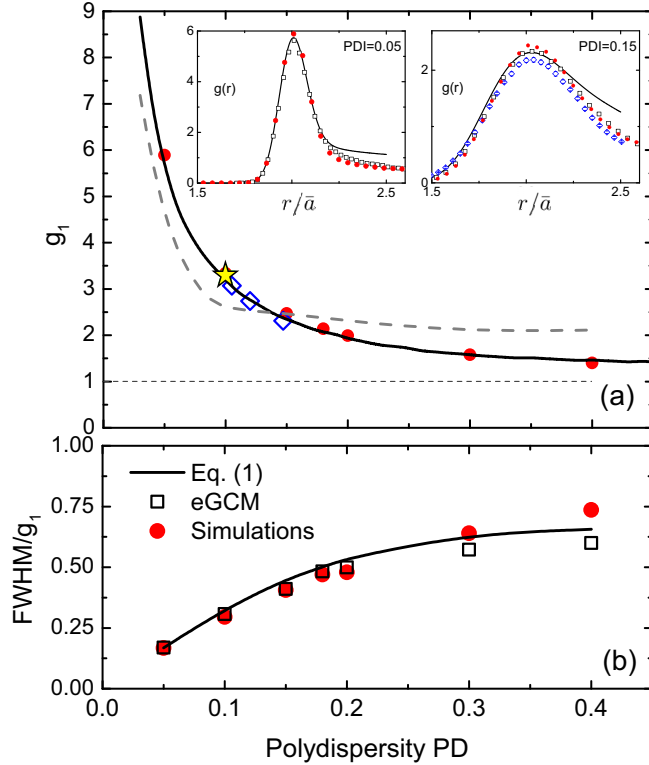


FIG. 5. (Color online) (a) Polydispersity dependence of the first peak value g_1 of the radial distribution function. The dashed line shows the prediction for g_1 obtained from packings numerically derived using the original GCM (neglecting rattlers) [26]. The solid line shows the prediction by Eq. (2). Diamonds: experimental results for polydisperse emulsions. Full circles: packing simulations. Star: experimental results for microgel particles, Ref. [29]. Inset: The first maximum of the radial distribution function $g(r)$ for a polydispersity $PD = 0.05$ (left) and $PD = 0.15$ (right). Prediction by Eq. (2) (solid line), the eGCM (open black squares), simulations (full red circles), and the emulsion experiments (open blue diamonds), $PD \simeq 0.15 \pm 0.01$. (b) Normalized FWHM.

We note that in practice, for a known polydispersity, $g(r)$ can be plotted directly using Eqs. (2) and (3) with input parameters \bar{N}_R, q taken from Fig. 3 and $s_{\text{cutoff}}/\bar{a} \sim 0.8$.

Finally, we illustrate briefly that the application of the eGCM is not restricted to log-normal particle size distributions. Other distributions such as Gaussian, linear, or bimodal can also be considered. A simple way to differentiate between these distributions is to introduce the skewness $S = \langle \delta a^3 \rangle / \langle \delta a^2 \rangle^{3/2}$ as an additional characteristic parameter. Recently published simulations have shown that the critical packing fraction ϕ_c depends both on the skewness and the polydispersity but is almost independent of other details of the shape of $p(a)$ [37]. In Fig. 6 we show a comparison between the eGCM predictions and these packing simulations reported in Ref. [37]. For clarity we restrict the discussion here to binary distributions. We find that for weak and moderate polydispersities both data sets agree well, while for extreme values of S and PD some deviations are observable. For linear distributions we obtain similar results (data not shown). The results for log-normal distribution are already shown in Fig. 3 and in this case polydispersity and skewness are

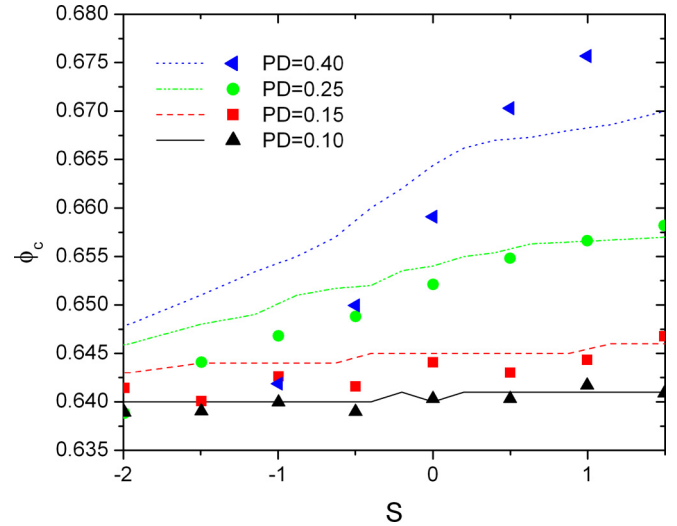


FIG. 6. (Color online) Critical volume fraction ϕ_c for binary particle size distributions with different polydispersity (PD), $\delta a/\bar{a}$, and skewness S . The lines denote predictions by the eGCM, and the full symbols represent the results from packing simulations taken from Ref. [37].

coupled. For truncated Gaussian distributions, $S \simeq 0$ for the weak-to-moderate polydispersities considered here.

V. SUMMARY AND CONCLUSIONS

In the present work, we have derived an extended granocentric model (eGCM) with the aim of providing a quantitative framework for modeling a bulk ensemble of polydisperse jammed spheres. Compared to the original approach [26,27], our improved model makes predictions for a number of key quantities that could not be treated within the original framework. The latter includes the radial distribution function $g(r)$ of all particles and the polydispersity-dependent critical jamming volume fraction ϕ_c . Many physical properties, such as the elastic modulus, can change very rapidly in the vicinity of ϕ_c , so even small changes in the ϕ_c predicted by various models can have an important impact on such observed physical properties. The main features of our approach can be summarized as follows. First, we have included noncontact neighbors, or rattlers, in our model, which we distribute uniformly as the simplest generalization. Second, we take into account size correlations between a chosen central particle and the particles in the shell [Eq. (1)]. This assumption is motivated by recent packing simulations [30]. Third, we allow the contact probability for added particles to depend on the residual available solid angle [Eq. (5)]. The latter is physically sound, and it is also required in order to obtain meaningful predictions for the jamming volume fraction ϕ_c for different polydisperse distributions. From an extensive comparison with experimental data and packing simulations, we demonstrate that our extended granocentric approach can deliver accurate predictions for a bulk ensemble of marginally jammed particles covering the full range of polydispersities of practical interest. Furthermore, we have tested the model for different skewed particle distributions and find good agreement with packing simulations [37]. The obtained quantitative modeling of $g(r)$ in turn provides a direct link between static structure factor

$S(q)$ and the structure of the packing. From a more general perspective the model can provide a framework for the interpretation of confocal microscopy, static and dynamic light-scattering experiments that can all be sensitive to the heterogeneities of the packing close to the jamming transition. A future extension of the model towards higher densities, taking into account finite particle compression, would open the path towards a full structural characterization of the bulk ensemble of polydisperse jammed particle systems.

ACKNOWLEDGMENTS

C.Z. and F.S. acknowledge financial support by the Swiss National Science Foundation (Project No. 149867). E.I.C. acknowledges the support of the NSF under CAREER Award No. DMR-1255370. M.M. and C.O. acknowledge financial support from the Science Foundation of Ireland, Grant No. 11/RFP.1/MTR/3135. We thank Eric Weeks and Ken Desmond for providing us with the original simulation data for the skewed distributions published in Fig. 2 of Ref. [37].

-
- [1] S. Torquato and F. Stillinger, *J. Phys. Chem. B* **105**, 11849 (2001).
- [2] S. C. Glotzer and M. J. Solomon, *Nature Mater.* **6**, 557 (2007).
- [3] L. Berthier, G. Biroli, J.-P. Bouchaud, L. Cipelletti, and W. van Saarloos, *Dynamical Heterogeneities in Glasses, Colloids, and Granular Media* (Oxford University Press, Oxford, UK, 2011).
- [4] Martin-D. Lacasse, G. S. Grest, D. Levine, T. G. Mason, and D. A. Weitz, *Phys. Rev. Lett.* **76**, 3448 (1996).
- [5] T. G. Mason, Martin-D. Lacasse, G. S. Grest, D. Levine, J. Bibette, and D. A. Weitz, *Phys. Rev. E* **56**, 3150 (1997).
- [6] S. Hutzler, R. P. Murtagh, D. Whyte, S. T. Tobin, and D. Weaire, *Soft Matter* **10**, 7103 (2014).
- [7] T. F. Tadros, *Emulsion Science and Technology* (Wiley-VCH, Weinheim, 2009), p. 1.
- [8] P. Stevenson, *Foam Engineering: Fundamentals and Applications* (John Wiley & Sons, New York, 2012).
- [9] D. Weaire and S. Hutzler, *The Physics of Foams* (Clarendon Press, Oxford, UK, 1999).
- [10] P. Coussot, *Rheometry of Pastes, Suspensions, and Granular Materials: Applications in Industry and Environment* (John Wiley & Sons, New York, 2005).
- [11] L. Mohan and R. T. Bonnecaze, *Soft Matter* **8**, 4216 (2012).
- [12] G. D. Scott, *Nature (London)* **188**, 908 (1960).
- [13] J. D. Bernal, *Nature (London)* **183**, 141 (1959).
- [14] A. J. Liu and S. R. Nagel, *Annu. Rev. Condens. Matter Phys.* **1**, 347 (2010).
- [15] M. Van Hecke, *J. Phys.: Condens. Matter* **22**, 033101 (2010).
- [16] T. S. Majmudar, M. Sperl, S. Luding, and R. P. Behringer, *Phys. Rev. Lett.* **98**, 058001 (2007).
- [17] I. Jorjadze, L.-L. Pontani, and J. Brujic, *Phys. Rev. Lett.* **110**, 048302 (2013).
- [18] Z. Zhang, N. Xu, D. T. Chen, P. Yunker, A. M. Alsayed, K. B. Aptowicz, P. Habdas, A. J. Liu, S. R. Nagel, and A. G. Yodh, *Nature (London)* **459**, 230 (2009).
- [19] F. Scheffold, F. Cardinaux, and T. G. Mason, *J. Phys.: Condens. Matter* **25**, 502101 (2013).
- [20] F. Scheffold, J. N. Wilking, J. Haberko, F. Cardinaux, and T. G. Mason, *Soft Matter* **10**, 5040 (2014).
- [21] P. Lindner and T. Zemb, *Neutron, X-rays and Light. Scattering Methods Applied to Soft Condensed Matter* (North-Holland, Amsterdam, 2002).
- [22] F. Scheffold and T. G. Mason, *J. Phys.: Condens. Matter* **21**, 332102 (2009).
- [23] M. Reufer, P. Diaz-Leyva, I. Lynch, and F. Scheffold, *The European Physical Journal E: Soft Matter and Biological Physics* **28**, 165 (2009).
- [24] M. Stieger, J. S. Pedersen, P. Lindner, and W. Richtering, *Langmuir* **20**, 7283 (2004).
- [25] T. G. Mason and D. A. Weitz, *Phys. Rev. Lett.* **74**, 1250 (1995).
- [26] M. Clusel, E. I. Corwin, A. O. Siemens, and J. Brujic, *Nature (London)* **460**, 611 (2009).
- [27] K. A. Newhall, I. Jorjadze, E. Vanden-Eijnden, and J. Brujic, *Soft Matter* **7**, 11518 (2011).
- [28] J.-P. Hansen and I. R. McDonald, *Theory of Simple Liquids* (Elsevier, New York, 1990).
- [29] T. A. Caswell, Z. Zhang, M. L. Gardel, and S. R. Nagel, *Phys. Rev. E* **87**, 012303 (2013).
- [30] C. B. O'Donovan, E. I. Corwin, and M. E. Möbius, *Philos. Mag.* **93**, 4030 (2013).
- [31] M. Wyart, *Ann. Phys. (Paris, Fr.)* **30**, 1 (2005).
- [32] P. K. Morse and E. I. Corwin, *Phys. Rev. Lett.* **112**, 115701 (2014).
- [33] J. Bibette, *J. Colloid Interface Sci.* **147**, 474 (1991).
- [34] J. Brujic, Experimental Study of Stress Transmission Through Particulate Matter, Ph.D. thesis, Cambridge University, 2004.
- [35] W. Press, B. Flannery, S. Teukolsky, and W. Vetterling, *Numerical Recipes in C* (Cambridge University Press, Cambridge, UK, 1995).
- [36] P. S. Mohanty, D. Paloli, J. J. Crassous, E. Zaccarelli, and P. Schurtenberger, *J. Chem. Phys.* **140**, 094901 (2014).
- [37] K. W. Desmond and E. R. Weeks, *Phys. Rev. E* **90**, 022204 (2014).